Voltammetric behavior of triethylamine trihydrofluoride and anisole in acetonitrile as a first approach of studies for electro-fluorination of some adducts

M.R. Ciumag[a], T. Tzedakis[a,*], C. André Barrès[b]

[a] *Laboratoire de Génie Chimique, UMR CNRS 5503, Université de Toulouse, UPS, 118 route de Narbonne, 31062 Toulouse, France*
[b] *Laboratoire de Synthèse et Physicochimie des Molécules à intérêt Biologique, UMR CNRS 5068, Université de Toulouse, UPS, 118 route de Narbonne, 31062 Toulouse, France*

A B S T R A C T

This work focuses on kinetic studies of anisole and triethylamine trihydrofluoride (fluorinating agent) on platinum electrode and acetonitrile as solvent, in order to get a better understanding of their anodic behavior. Results show that both compounds can be oxidized and some kinetic parameters are calculated: the diffusion coefficient within the working media, the anodic electronic transfer coefficient and the apparent intrinsic heterogeneous electronic transfer constant. An unusual variation of these parameters occurs within the chosen reaction conditions, particularly by varying the triethylamine trihydrofluoride concentration. Preliminary experiments for anodic fluorination of dimethoxy ethane (DME) and anisole were carried out and even if results show a possible electrofluorination for the DME (classically used as solvent), there is no fluorination of anisole when electrochemical microreactor was used.

1. Introduction

Fluoride chemistry is important in various fields: one agro-biological molecule of two has at least one fluoride atom; for the pharmaceutical domain the proportion is one to three. It is also important to note the use of ^{18}F, fluoride artificial isotope, in medical imagistic for positron emission topography, to diagnose neuro-degenerative cerebral disease (epileptic, Parkinson) or tumors.

Fluoride characteristics, e.g. its strong electro-negativity, can significantly modify the physico-chemical properties of a molecule; this makes fluorination to be difficult and shows the need for new synthesis methodologies and new more efficient fluorinating agents. Chemical fluorination of various molecules involves multi-step reaction process, using gaseous fluorine ("Shiemann and Halex" in the industrial scale, toluene fluorination). For reducing the risks, several electrochemical studies [1–12] were carried out, on the anodic fluorination. General conclusions of these works, expressed in terms of fluorination yield, selectivity, number and position in the final product of fluoride atoms, shown the difficulty to fluorinate alkylated groups in alpha position of a hetero-atom, and inform on the optimal conditions (electrolyte nature, solvents, electrode material and electric energy to provide), to choose. Nevertheless, in our knowledge, there are not any electrode kinetic studies considering mixtures of compounds to fluorinate in presence of fluorination agent.

Suryanarayanan and Noel [1] have shown that electrolytes such as $Et_3NF{\cdot}4HF$, $Et_3N{\cdot}3HF$ in solvents such as dimethoxyethane, dimethylformamide or acetonitrile act like nucleophylic fluorinating agents, conditioning the selectivity of anodic fluorination process. Selective electrochemical fluorination of indanone compounds was also carried out in $Et_4NF{\cdot}3HF$ used as Ionic liquid solvent.

Fuchigami is one of the authors who most studied the organic compounds fluorination [2–8]. Amines like $Et_3N{\cdot}5HF$ and $Et_4NF{\cdot}4HF$ were used as electrolyte and fluorinating agent by Hou and Fuchigami for ethyl α-(2-pyrimidylthio) acetate [2], for diethylene glycol dimethyl ether or dimethoxyethane [3] as well as for flavones compounds fluorination [4]; fluorination yield can reach 98%, nevertheless 8F/mol of substrate are required.

Baba et al. [5] studied thioazolidins fluorination in dimethoxyethane, in presence of fluorinated salts. The yield in mono-fluorinated product depends on the solvent: in the case of acetonitrile, conversion increases with the number (n) of HF in $Et_3N{\cdot}nHF$ molecule. Suzuki et al. [6] studied 4-phenylthyomethyl-1,3-dioxolane-2-one fluorination in presence of $Et_3N{\cdot}3HF$ as electrolyte and dimethoxyethane, dichloromethane and acetonitrile as solvents; meanwhile with dimethoxyethane only the mono-fluorinated product is obtained, the use of acetonitrile allows high difluorination yields. Let us note that even if frequently

* Corresponding author. Tel.: +33 561558302; fax: +33 561556139.
E-mail address: tzedakis@chimie.ups-tlse.fr (T. Tzedakis).

Nomenclature

c and c^0	concentration and initial concentration (mol L^{-1})
CE	counter or auxiliary electrode
D	diffusion coefficient (m^2 s^{-1})
E, E^0, $E^{0'}$	potential, standard potential and apparent standard potential (V)
$Et_3N{\cdot}3HF$	triethylamine trihydrofluoride
F	Faraday constant (96,480 C mol^{-1})
I, I_{peak}, I_k	current, peak current, and current free of mass-transfer effects (A)
K	triethylamine trihydrofluoride adsorption equilibrium constant (concentration in mol L^{-1})
$k^{0'}$ and k^0	apparent intrinsic, and intrinsic heterogeneous electronic transfer constants (m s^{-1})
n_{gl}	global number of exchanged electrons
n_{ls}	number of electrons exchanged within the limiting step
r	potential scan rate (V s^{-1})
R	ideal gas law constant (8.31 J mol^{-1} K^{-1})
S	working electrode geometrical surface (m^2)
T	absolute temperature (K)
α	anodic electronic transfer coefficient
Γ and Γ_{max}	interfacial concentration and interfacial concentration at saturation (mol m^{-2})
θ	coverage ratio
ν	kinematic viscosity (assumed to be the acetonitrile viscosity: 4.25×10^{-4} m^2 s^{-1})
ω	angular velocity (RPM or rad s^{-1}).

used as fluorinating agents, there is no available information about the fluorinated triethylamines electrochemical behavior, or kinetic parameters.

Ishii [8] shows that acidity difference between hydrogen atoms substituted at the oxygen or at the methyl carbon (e.g. dimethoxyethane), makes the substitution to occur at the hydrogen atom of the carbonyl group, i.e. the alpha position (the most expected) of the C—O bound.

$Et_3N{\cdot}4HF$ and fluorohydric acid, even if very corrosive, were also used as fluorinating agents by Ilayaraja et al. [9,10]; for dimethyl glutarate fluorination, monofluoro dimethyl-glutarate were obtained with a 71% yield for a 6F/mol charge.

This preliminary work presents electrochemical kinetic studies, first expecting the understanding of anisole electrochemical behavior in presence or absence of the triethylamine trihydrofluoride, used both as fluorinating agent and electrolyte. On the other hand, the works carried out aim to help to approach the final goal of our study, the direct anodic fluorination of valuable adducts (e.g. anisole) using an electrochemical microreactor, appropriated to this kind of reactions [13–16].

2. Experimental

Analytical degree products were provided by Sigma–Aldrich (dimethoxyethane and acetonitrile as solvents), and by Acros Organics (tetrabutylammonium perchlorate and tetraethylammonium perchlorate as electrolytes, anisole and trifluorinated amine). An Autolab 30 potentiostat-galvanostat (GPES software) and a classical thermoregulated 'three-electrodes' electrochemical cell were used. The working electrode was a gold or platinum rotating disk (r = 1 mm), cleaned before each experiment. The counter-electrode was a platinum wire and the reference was a SCE.

3. Results

3.1. Electrochemical study of triethylamine trihydrofluoride ($Et_3N{\cdot}3HF$) on gold anode

Transient state current–potential curves were plotted in order to study the influence of the potential scan rate and concentration on the triethylamine trihydrofluoride oxidation.

Fig. 1(a) shows results obtained for a solution containing 0.1 mol L^{-1} of triethylamine trihydrofluoride $Et_3N{\cdot}3HF$, used both as supporting electrolyte and fluorinating agent, in dimethoxyethane (DME) solvent. A plateau appears (instead of a peak) in the range 0.2–1 V vs SCE, attributed to the triethylamine trihydrofluoride oxidation. For potentials higher than 1.5 V vs SCE, the exponential shape of the curve translates a pure activation limitation, and this signal could be attributed to the solvent or the gold electrode oxidation. The current magnitude increases with the potential scan rate and shifts towards more anodic potentials. For a higher $Et_3N{\cdot}3HF$ concentration (1 mol L^{-1}), the plateau appears (Fig. 1(b)) in the range of 1–1.5 V vs SCE, and tends to become a peak when the potential scan rate increases.

By examining the electrode surface at the end of the experiments one can observe corrosion of the gold anode. In absence of the fluorinated agent no corrosion takes place. Fluoride anion arising from triethylamine trihydrofluoride dissociation decrease the gold oxidation potential and cause the anodic oxidation of this material (second signal (E > 1.5 V).

Current–potential curves are also plotted using acetonitrile (CH_3CN) as solvent, tetraethylammonium perchlorate (Et_4NClO_4) as electrolyte and triethylamine trihydrofluoride ($Et_3N{\cdot}3HF$) as fluorinating agent. A similar behavior was observed for both curve shapes and gold surface corrosion, as in the case of dimethoxyethane.

One can conclude that the gold electrode is not appropriate for this study because of its instability; a platinum electrode will be used as working electrode for the further study of fluorination reactions.

3.2. Electrochemical study of tri-fluorinated ($Et_3N{\bullet}3HF$) triethylamine on platinum anode

3.2.1. Influence of the triethylamine trihydrofluoride concentration

The electrochemical behavior of $Et_3N{\cdot}3HF$ was studied in acetonitrile containing Bu_4NClO_4 0.2 mol L^{-1}, in order to have a better understanding of its anodic oxidation process. Potential current curves (Fig. 2) obtained for various $Et_3N{\cdot}3HF$ concentrations show two signals at 0.9 V/1.7 V and 2.2 V/3 V vs SCE.

By analyzing the variation of the current magnitude of the first signal (1.5/1.7 V vs SCE), versus the $Et_3N{\bullet}3HF$ concentration, for three potential scan rates (Fig. 3(a)), one can observe the appearance of a plateau for $Et_3N{\cdot}3HF$ concentrations higher than 2×10^{-2} mol L^{-1}. This behavior could be due to the triethylamine trihydrofluoride adsorption on the platinum surface.

Because of the low electrode area, the adsorbed quantity of $Et_3N{\cdot}3HF$ could be assumed negligible, consequently its concentration in the bulk can be assumed constant.

A Langmuir isotherm model was expected to govern $Et_3N{\cdot}3HF$ adsorption, and following analysis aims to demonstrate this assumption.

$$Et_3N \cdot 3HF + \text{adsorption site}\,(\sigma) \underset{k_b}{\overset{k_f}{\rightleftarrows}} (Et_3N \cdot 3HF)_{adsorbed} \quad (1)$$

The interfacial concentration Γ of the adsorbed free $Et_3N{\cdot}3HF$ can be expressed (using the coverage ratio θ (2)), according the Langmuir model (3).

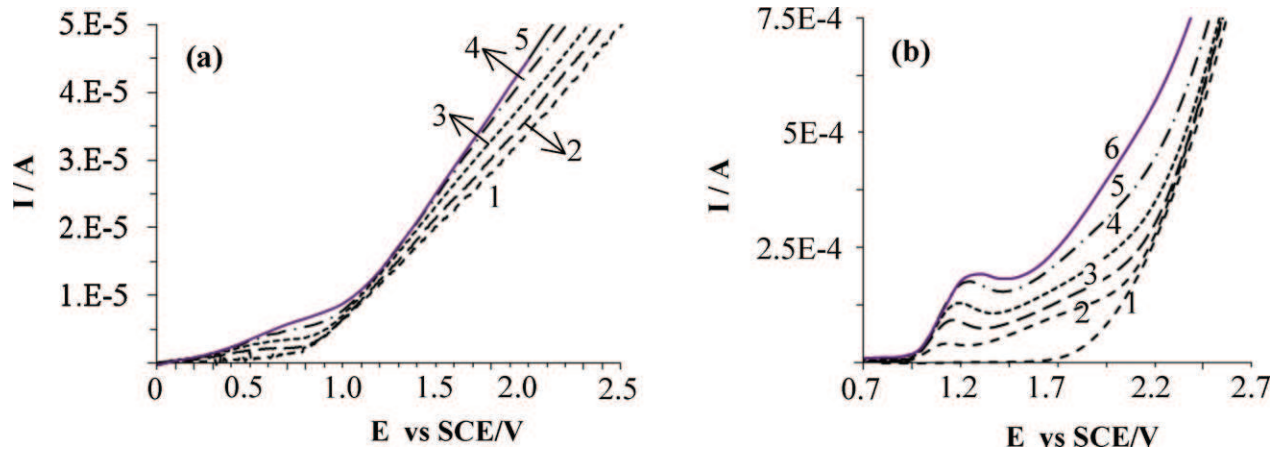

Fig. 1. Potential scan rate dependency on the current–potential curves, obtained on gold rotating disk electrode (r = 1 mm) immersed in dimethoxyethane solvent containing tri-fluorinated triethylamine in two concentrations: (a) $Et_3N{\cdot}3HF$ 0.1 mol L^{-1}; (b) $Et_3N{\cdot}3HF$ 1 mol L^{-1}. CE: Pt; 25 °C; no stirring. Curves 1–6: 0, 0.05, 0.1, 0.2, 0.5 and 1.0 V s^{-1} respectively.

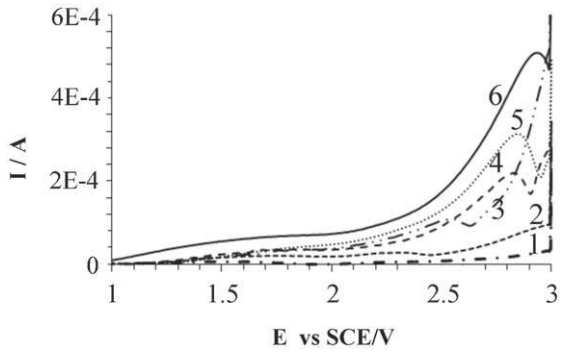

Fig. 2. Current–potential curves obtained for different tri-fluorinated triethylamine concentrations, on platinum disk electrode (r = 1 mm) immersed in acetonitrile solvent containing Bu_4NClO_4 0.2 mol L^{-1}; CE: Pt; 25 °C; r = 0.1 V s^{-1}; no stirring. Curves 1–6: $Et_3N{\cdot}3HF$ 10^{-3}, 8×10^{-3}, 2×10^{-2}, 3.5×10^{-2}, 5×10^{-2} and 7×10^{-2} mol L^{-1} respectively.

$$\theta = \frac{[\text{occupied sites}]}{[\text{available sites}]} = \frac{\text{interfacial concentration } \Gamma\,(\text{mol m}^{-2})}{\text{interfacial concentration at saturation } \Gamma_{\max}\,(\text{mol m}^{-2})} \quad (2)$$

$$\Gamma = \frac{K\Gamma_{\max}c}{1+KC} \quad (3)$$

where K is the adsorption equilibrium constant = k_f/k_b and c is the free $Et_3N{\cdot}3HF$ concentration, i.e. its initial concentration.

The curves in Fig. 2 (as well as curves in Fig. 6, next section) show that $Et_3N{\cdot}3HF$ is an irreversible system: the potential of the second signal shifts towards more anodic values with triethylamine trihydrofluoride concentration. Consequently, the peak current magnitude for a monolayer adsorbed species can be expressed [17] by relation (4).

$$I_{\text{peak}} = \frac{n_{\text{gl}}\cdot n_{\text{ls}}\cdot\alpha\cdot F^2\cdot r\cdot\Gamma\cdot S}{2.718\cdot R\cdot T} \quad (4)$$

where n_{gl} is the global number of exchanged electrons, n_{ls} is the number of electrons exchanged within the limiting step, α is the anodic electron transfer coefficient, F is the Faraday constant (96480 C mol^{-1}), r is potential scan rate (V s^{-1}), S is the working electrode geometrical area (m^2), T is the absolute temperature (K) and R is the gas constant (8.31 J mol^{-1} K^{-1}).

Combination of Eqs. (3) and (4) led to relation (5), allowing the access to the adsorption equilibrium constant K.

$$\frac{1}{I_{\text{peak}}} = \frac{1}{\mu} + \frac{1}{\mu\cdot K\cdot c} \quad (5)$$

where

$$\mu = \frac{n_{\text{gl}}\cdot n_{\text{ls}}\cdot\alpha\cdot F^2\cdot r\cdot S\cdot\Gamma_{\max}}{2.718\cdot R\cdot T}$$

Fig. 3(b) shows the linear dependence of the current reverse against the reverse of $Et_3N{\cdot}3HF$ initial concentration, which is in agreement with the Langmuir model. Assuming: n_{gl} = 2 (per mole of produced fluorine), n_{ls} = 1 and α = 0.5, one can estimate from the previous results the $Et_3N{\cdot}3HF$ adsorption equilibrium constant K, as well as the number of sites available to adsorption $\Gamma_{\max}$.

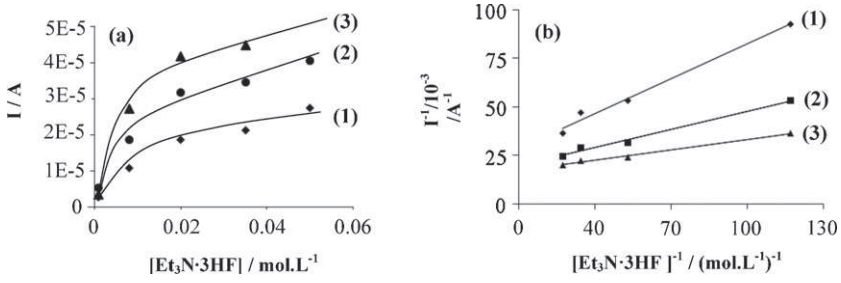

Fig. 3. $Et_3N{\cdot}3HF$ concentration influence on the current of the signal located in the potential range from 1.5 to 1.7 V vs SCE. Curve (2) was obtained from Fig. 2; curves (1) and (3) were obtained from other I/E curves, represented in the next section or no represented here. (1)–(3): 0.01, 0.10 and 0.20 V s^{-1}, respectively. (a): $I_{\text{signal at 1.5–1.7 V}} = f([Et_3N{\cdot}3HF])$ for different potential scan rates; (b): $(I_{\text{signal at 1.5–1.7 V}})^{-1} = f(\{[Et_3N{\cdot}3HF]\}^{-1})$ for different potential scan rates.

Table 1
Results obtained from Fig. 3(b), on the first anodic signal of the tri-fluorinated triethylamine, related to its adsorption on the platinum anode.

Potential scan rate, r ($V\,s^{-1}$)	$\{I_{signal\ at\ 1.5–1.7\,V}\}^{-1} = \xi + \psi/[Et_3N{\cdot}3HF]$		R^2	K (concentration was expressed in $mol\,L^{-1}$)	Γ_{max} ($\times 10^{-4}$ $mol\,m^{-2}$)
	ξ (A^{-1})	ψ ($(mol\,L^{-1})^{-1}$)			
0.01	33.6×10^3	420	0.988	80	6.6
0.10	22.4×10^3	215	0.990	104	1.3
0.20	17.0×10^3	212	0.991	65	0.6

The average estimated equilibrium constant for the $Et_3N{\bullet}3HF$ adsorption at 25 °C is: $K = (0.8 \pm 0.2) \times 10^2$, a relatively low value demonstrating a relatively low affinity of this compound for the platinum anode. The interfacial concentration at saturation (Γ_{max}) of the $Et_3N{\cdot}3HF$ adsorbed on platinum decreases when the potential scan rate increases (Table 1), indicating an unusual behavior of an adsorbed species.

However, the first signal appears to be a peak for the lower concentrations (Fig. 2, curves 1–4), while increasing the concentration (Fig. 2, curves 5 and 6), causes the shape of the signal to become a plateau with practically constant current, similar to a limiting current. The limiting current is in accordance with a no limitative adsorption step, meaning a rapid establishment of the adsorption equilibrium, because the higher concentration of the $Et_3N{\cdot}3HF$ in the bulk. This opposite behavior will be discussed in the next sections, because other phenomena could take place.

Indeed $Et_3N{\cdot}3HF$ is a complex resulted from association of hydrofluoric acid and Et_3N according to an equilibrium. Nevertheless, a study performed by ^{19}F NMR on the stability of $Et_3N{\cdot}3HF$ 1M in acetonitrile (Fig. 4), showed that resulting complex seem to be instable. Obtained spectra show that the signal of $Et_3N{\cdot}3HF$ (−87 ppm/CF_3COOH) completely disappears after 16 h, and four additional signals appears (−74, −73, −66 and −48 ppm). It seems that $Et_3N{\cdot}3HF$ decomposes to various products ($Et_3N{\cdot}2HF$, $Et_3N{\cdot}HF$, Et_3N and hydrofluoric acid). A similar behavior was observed for other solvents.

On the other hand, studies of Fuchigami et al. [2–4] shown that when fluorination was carried out using $Et_3N{\cdot}3HF$, at the end of the reaction free Et_3N was detected, meaning that the complex dissociates during the fluorination.

The second $Et_3N{\cdot}3HF$ oxidation signal (Fig. 2) appears to be a peak located in the range of 2.2 V/3 V vs SCE; its current magnitude

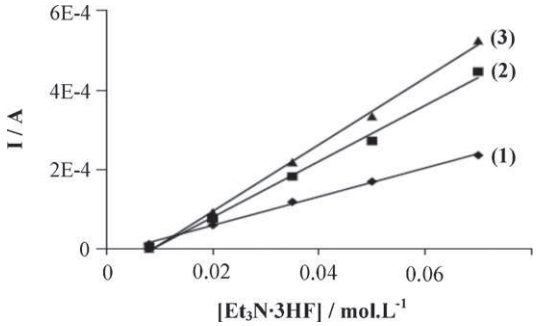

Fig. 5. Current magnitude dependence of $Et_3N{\cdot}3HF$ concentration for the second oxidation signal (curves of Fig. 2), located in the range 2.2–3 V vs SCE. (1)–(3): 0.01, 0.10 and 0.20 $V\,s^{-1}$ respectively.

shows a linear dependence against the triethylamine concentration (Fig. 5), meaning a diffusion limited reaction. The intercept of theses straight lines is not zero, because the residual current was not removed; indeed, blank elimination is difficult because the $Et_3N{\cdot}3HF$ act both as electrolyte and electroactive species, influencing the migration current and causing changes in the blank.

In addition, this signal shifts towards more anodic potentials and its peak potential seems to be strongly influenced by $Et_3N{\cdot}3HF$ concentration (Fig. 2), probably because of pH variation induced by a partial decomposition of $Et_3N{\cdot}3HF$, leading to fluorohydric acid.

In conclusion, triethylamine trihydrofluoride can be oxidized both as an adsorbed and free forms. Adsorption on platinum electrode obeys to the Langmuir isotherm model, while the second electrochemical signal translates a mass transfer limitation.

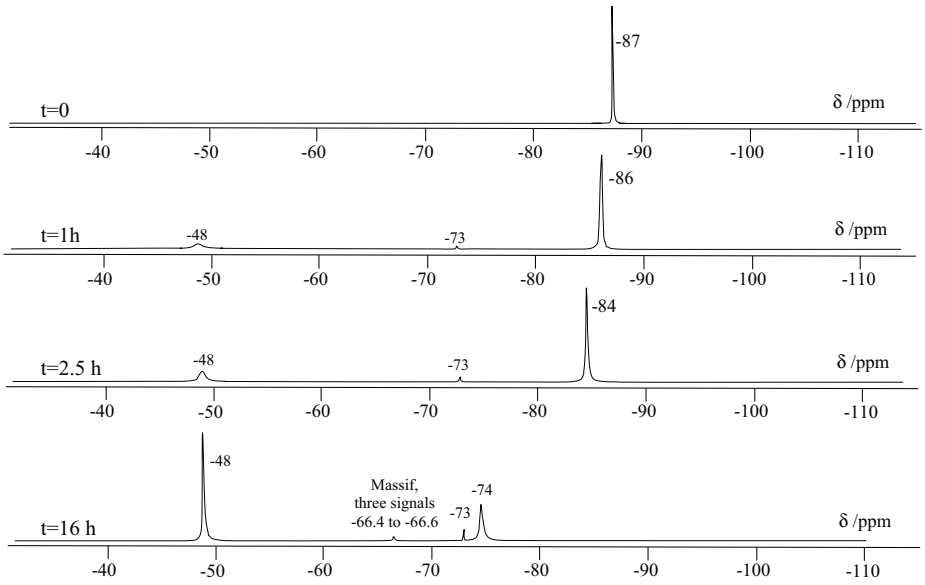

Fig. 4. Stability of a $Et_3N{\cdot}3HF$ solution at 1 mol/L in acetonitrile, followed by ^{19}F NMR. Reference CF_3COOH at 0 ppm; signal of CF_3COOH: −77 ppm vs $CFCl_3$.

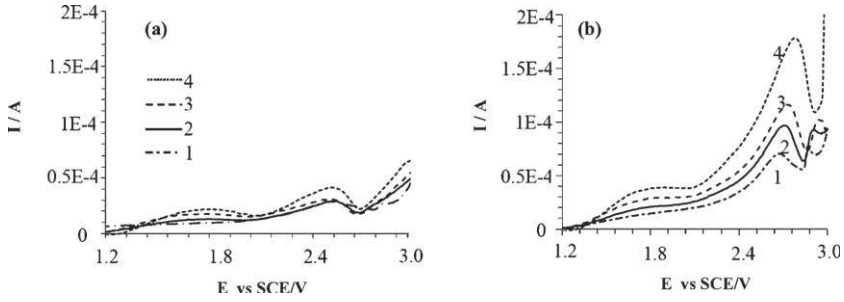

Fig. 6. Current–potential curves obtained for various potential scan rates, on platinum disk anode ($r = 1$ mm) immersed in acetonitrile containing Bu_4NClO_4 0.2 mol L^{-1}; CE: Pt; 25 °C; no stirring. 1–4: 0.017, 0.083, 0.170 and 0.500 V s^{-1} respectively. (a) $Et_3N{\cdot}3HF$ 8×10^{-3} mol L^{-1}; (b) $Et_3N{\cdot}3HF$ 2×10^{-2} mol L^{-1}.

3.2.2. Influence of the potential scan rate on the triethylamine trihydrofluoride oxidation

In order to access to the $Et_3N{\bullet}3HF$ kinetic parameters, its electrochemical behavior in the acetonitrile–Bu_4NClO_4 media was studied (Fig. 6), by plotting the current potential curves for various potential scan rates. As previously (Fig. 2), the current–potential curves obtained for different potential scan rates show the adsorption wave (mainly present in the expected form, i.e. a peak) followed by the diffusion peak.

For the first signal, a linear dependence (6) of the potential scan rate on the current magnitude, according to relation (4), was obtained and confirms the electrochemical reaction limitation by the $Et_3N{\cdot}3HF$ adsorption on the electrode surface.

$$I_{peak} = 0.121 + 0.0183r, \quad R^2 = 0.989 \tag{6}$$

The intercept of this relation is not zero, because the residual current was not removed (same reason as in the case of Fig. 5).

The peak potential of the second signal (2.6–2.8 V vs SCE, Fig. 6) shifts towards more anodic values when the potential scan rate increases; its variation versus the natural logarithm of the scan rate, according to the relation (7), allows having some information about the system reversibility/irreversibility:

$$E_{peak} = E^{0'} + \frac{R \times T}{\alpha \times n_{ls} \times F}\left[0.78 + \ln\frac{D^{1/2}}{k^0} + \ln\left(\frac{\alpha \times n_{ls} \times F \times r}{R \times T}\right)^{1/2}\right] \tag{7}$$

where $E^{0'}$ is the apparent standard potential of the electroactive system (V) and k^0 is the intrinsic heterogeneous electronic transfer constant (m s^{-1}).

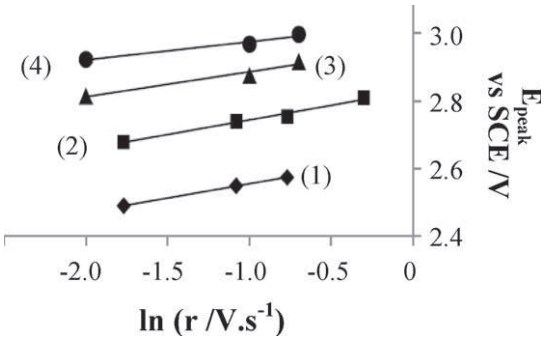

Fig. 7. Second anodic peak potential variation against the logarithm of the potential scan rate for various $Et_3N{\cdot}3HF$ concentrations. Results from Fig. 6 and other curves not presented. Curves 1–4: $Et_3N{\cdot}3HF$ 8×10^{-3}, 2×10^{-2}, 3.5×10^{-2} and 7×10^{-2} mol L^{-1} respectively.

Results for $Et_3N{\cdot}3HF$ concentrations in the range 8×10^{-3} to 7×10^{-2} mol L^{-1} (Fig. 7) show a linear correlation, meaning that the electroactive system is irreversible.

The average value of slopes obtained in Table 2 ($\bar{x} = 2.303\,(RT/2\alpha n_{ls}F)$) allows estimating $\overline{\alpha n_{ls}} \sim 0.36$.

One can observe that an increased $Et_3N{\cdot}3HF$ concentration does not affect the slope, while the intercept increases. Changes in the intercept value (Table 2) with the $Et_3N{\cdot}3HF$ concentration are an unclassical observation and they will be discussed at the end of this paragraph.

Taking into account the αn_{ls} value determined previously, the $Et_3N{\cdot}3HF$ diffusion coefficient can be determined using the linear dependence of the potential scan rate square root with the current magnitude (8) and results for four $Et_3N{\cdot}3HF$ concentrations are indicated in Table 3.

$$I_{peak} = 2.99 \times 10^5 \cdot n_{gl} \cdot \sqrt{\alpha \cdot n_{ls} \cdot D} \cdot S \cdot c^0 \cdot \sqrt{r} \tag{8}$$

where D is the $Et_3N{\cdot}3HF$ diffusion coefficient in CH_3CN containing Bu_4NClO_4 0.2 mol L^{-1} (m^2 s^{-1}); c^0 is the triethylamine trihydrofluoride initial concentration in the bulk (mol L^{-1}); $n_{gl} = 2$ (per mole of produced fluorine).

The relative good linearity of the four curves $I_{peak} = f(\sqrt{r})$ confirms the kinetics limitation by the $Et_3N{\cdot}3HF$ diffusion. Nevertheless, determined $Et_3N{\cdot}3HF$ diffusion coefficient slightly ($(2.85 - 1.24)/2.85 = 0.56$) changes with concentration, a logarithmic increase of this parameter was observed (Fig. 8), relation (9):

$$D_{Et_3N{\cdot}3HF}\ (m^2\ s^{-1}) = 4.77 \times 10^{-10} + 7.29 \times 10^{-11} \cdot \ln[Et_3N \cdot 3HF]\ (\text{mol } L^{-1}), \quad R^2 = 0.995 \tag{9}$$

This variation, even if not important, seems unusual. A possible reason explaining this change could be the migration current. Indeed,

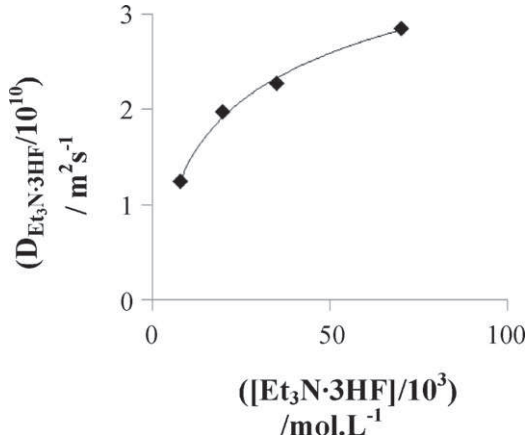

Fig. 8. $Et_3N{\cdot}3HF$ diffusion coefficient variation with initial tri-fluorinated triethylamine concentration.

Table 2
Results obtained from Fig. 7, on the second anodic signal of the tri-fluorinated triethylamine, related to its diffusion-controlled nature.

$[Et_3N{\cdot}3HF]$ (mol L^{-1})	E_{peak} (V) = $\phi + x\log(r)$ (V s^{-1}) according to relation (7)			R^2	αn_{ls}	$\overline{\alpha n_{ls}}$
	ϕ	x	$\bar{x}$			
8×10^{-3}	2.639	0.084	0.0805	0.999	0.35	0.36
2×10^{-2}	2.830	0.087		0.984	0.34	
3.5×10^{-2}	2.960	0.074		0.965	0.39	
7×10^{-2}	3.048	0.077		0.969	0.37	

because the chosen TBAP concentration (0.2 mol L^{-1}), the ions arising from $Et_3N{\cdot}3HF$ dissociation, especially F^-, could migrate and consequently increase the migration anodic current, which cannot be neglected in the whole examined range of $Et_3N{\cdot}3HF$ concentration: 8×10^{-3}–2×10^{-2} mol L^{-1}.

The transference number of the electroactive species, $t_{Et_3N{\cdot}3HF}$ can be estimated according follow relation:

$$t_{Et_3N{\cdot}3HF} = \frac{z^2_{\text{anion arises from } Et_3N{\cdot}3HF \text{ dissociation}} \times F^2 \times u_{\text{anion arises from } Et_3N{\cdot}3HF \text{ dissociation}} \times [Et_3N \cdot 3HF]}{\sum_{\text{all ions } j} z_j^2 \times F^2 \times u_j \times [j]}$$

Because we do not know mobility of ions arising from these electrolytes in acetonitrile, we will use the following approximations:

- both TBAP and $Et_3N{\cdot}3HF$ are assumed to be binary electrolytes,
- mobilities u_j of all j ions arising from these electrolytes have the same order magnitude.

The transference number can be written as follow:

$$t_{Et_3N{\cdot}3HF} = \frac{[Et_3N \cdot 3HF]}{2 \times [Et_3N \cdot 3HF] + 2 \times [TBAP]}$$

and its values (Table 3), in the range from 0.01 to 0.13, are relatively low.

Note that these values are simple estimations, because the dissociation of $Et_3N{\bullet}3HF$ is partial and the concentration of the arising anion is lower than the $Et_3N{\bullet}3HF$ concentration used to estimate the transference number. In these conditions, the estimated transference number is higher than the real one.

For a binary electrolyte, the product $(1/(1-t_j))$ translates the contribution of the ion j migration flux, in the diffusion flux of this ion. Consequently, relation (8) can be rewritten:

$$I_{peak} = \frac{1}{1-t_j} \cdot 2.99 \times 10^5 \cdot n_{gl} \cdot \sqrt{\alpha \cdot n_{ls} \cdot D} \cdot S \cdot c^0 \cdot \sqrt{r} \qquad (8bis)$$

Using the relation (8bis), an estimation of the $Et_3N{\cdot}3HF$ diffusion coefficient taking into account the migration current was proposed and results are indicated in Table 3. As previous, obtained values of D change with $Et_3N{\cdot}3HF$ concentration; nevertheless:

- differences in the D values, are in a narrow range (1.1×10^{-10} to 2.2×10^{-10}) instead 1.2×10^{-10} to 2.8×10^{-10} e.g. $((2.2-1.1)/2.2 = 0.5)$,
- effect of the migration term is relatively low: $6\% < \Delta\{(D_D - D_{M/D})/D_D\} < 22\%$.

The variation of D vs concentration seems unusual, as passivation problems could not explain it completely. Increased $Et_3N{\cdot}3HF$ concentration leads to a more important passivation and consequently, causes current and diffusion coefficient to decrease. As explained above, $Et_3N{\cdot}3HF$ can decompose in free fluorohydric acid and triethylamine; either $Et_3N{\cdot}3HF$ and HF oxidation could be attributed to the obtained signal. Thus determined D using the slope of relation (8bis) is an apparent diffusion coefficient because the value of the initial concentration was used instead the real concentration of the corresponding electroactive species (which is lower one the initial concentration)

Diffusion coefficient variation versus the concentration of $Et_3N{\cdot}3HF$ can also (partially) explain the changes on the intercept value (Table 2) previously observed. Consequently, determination of the intrinsic heterogeneous electronic transfer constant k^0 seems to be difficult because both the concentration of the electroactive species and the $E^{0'}$ value are unavailable. One will try to access to this parameter in the next section.

3.2.3. *Influence of the angular velocity of the platinum anode on the triethylamine trihydrofluoride oxidation*

In order to better understand this system, (estimation of k^0, comparison of the results for D), current–potential curves were plotted at the steady state, for various $Et_3N{\cdot}3HF$ concentrations and angular velocities of a rotating platinum disk. Results (Fig. 9) show a similar shape curve for all the examined concentrations. The current magnitude for the first oxidation signal (1.2–2 V vs SCE), previously attributed to the $Et_3N{\cdot}3HF$ adsorption on the electrode surface, seems to be affected by the stirring, for the low examined concentrations (Fig. 9(a) and (b)); no effect was observed for higher concentrations: (Fig. 9(c) and (d)).

Theoretically, adsorption is not affected by stirring. Nevertheless, a slow adsorption rate can influence the time required to reach the equilibrium. For a $Et_3N{\cdot}3HF$ concentration high enough, the adsorption equilibrium is rapidly reached and the stirring does not affect the curves. Conversely, for concentrations up to 2×10^{-2} mol L^{-1}, the time necessary to saturating the electrode is higher and the stirring can have an effect. The low value of $Et_3N{\cdot}3HF$ adsorption equilibrium constant (K) and the Γ_{max}

Table 3
$Et_3N{\cdot}3HF$ diffusion coefficient calculated with relation (8) and αn_{ls} values from Table 2; $n_{gl} = 2$. Results obtained from Fig. 6.

$[Et_3N{\cdot}3HF]$ (mol L^{-1})	Slope $I_{peak\ at\ 2.6/2.8\ V} = f(r^{1/2})$	R^2	$D_{Et_3N{\cdot}3HF}$ ($\times 10^{10}$ m^2 s^{-1}) (without migration contribution to the current)	Estimated transference number of $Et_3N{\cdot}3HF$, $t_{Et_3N{\cdot}3HF} = [Et_3N \cdot 3HF]/(2[Et_3N \cdot 3HF] + 2[TBAP])$	$D_{Et_3N{\cdot}3HF}$ ($\times 10^{10}$ m^2 s^{-1}) (with migration contribution to the current)	$\Delta\frac{D_D - D_{M/D}}{D_D}$ (%)
8×10^{-3}	9.91×10^{-5}	0.964	1.24	0.02	1.16	6.3
2×10^{-2}	3.08×10^{-4}	0.982	1.97	0.04	1.70	13.7
3.5×10^{-2}	6.18×10^{-4}	0.998	2.27	0.07	2.10	7.5
7×10^{-2}	1.35×10^{-3}	0.989	2.85	0.13	2.21	22.4

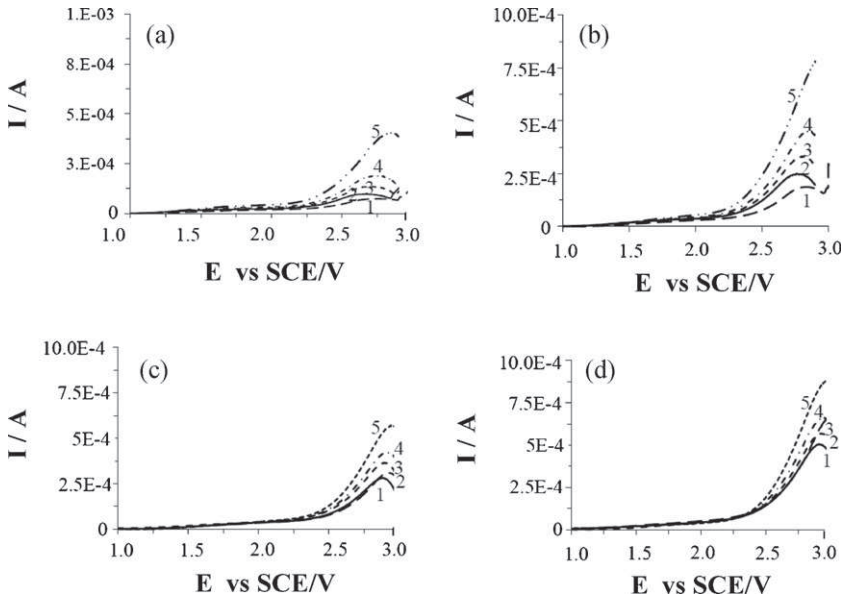

Fig. 9. Angular velocity (ω) dependence of the current–potentials curves obtained on platinum rotating disk (r = 1 mm), immersed in acetonitrile solvent, containing Bu_4NClO_4 0.2 mol L^{-1}; CE: Pt; $r = 4 \times 10^{-3}$ V s^{-1}; 25 °C. Curves 1–5: ω = 100 rpm, 250 rpm, 500 rpm, 1000 rpm and 5000 rpm respectively. (a) $Et_3N{\cdot}3HF$ 8×10^{-3} mol L^{-1}; (b) $Et_3N{\cdot}3HF$ 2×10^{-2} mol L^{-1}; (c) $Et_3N{\cdot}3HF$ 3.5×10^{-2} mol L^{-1}; (d) $Et_3N{\cdot}3HF$ 7×10^{-2} mol L^{-1} respectively.

variation with the potential scan rate (Table 1), are in accordance with these results.

Another reason that could explain this behavior is represented by a temperature variation at the electrode surface, arising from $Et_3N{\cdot}3HF$ decomposition, a phenomenon damped by the stirring.

The second oxidation signal appears to be a peak and its potential shifts to more anodic values (~2.3 to ~3 V vs SCE) when the $Et_3N{\cdot}3HF$ concentration increases, fact that confirms its irreversible behavior. For a classical electroactive system, this 'diffusion limited' signal, at the steady state, has to show a limiting current plateau; the obtained 'peak'-shaped curve translates passivation phenomena caused by a thin layer of gaseous fluorine produced at the electrode surface. Using the 'net/exempted of the blank' maximum current of this signal, as an approximation for the expected limiting current (Fig. 9), linear correlations (Table 4) were obtained for the four $Et_3N{\cdot}3HF$ concentrations, following Levich relation:

$$I_{lim} = 0.62 \cdot n_{gl} \cdot F \cdot S \cdot D^{(2/3)} \cdot c^0 \cdot \nu^{-(1/6)} \cdot \sqrt{\omega} \quad (10)$$

where n_{gl} is assumed to be 2 (by molecule of produced F_2), ω is the electrode angular velocity (rad s^{-1}) and ν is the media kinematic viscosity, assumed to be the acetonitrile viscosity (4.25×10^{-4} m^2 s^{-1}).

The linear correlation $I_{lim} = f(\sqrt{\omega})$ obtained, could mean that passivation does not strongly affect the electrode surface, because a strong stirring could contribute to remove bubbles from the electrode surface. Slopes of the four curves allow estimation of triethylamine trihydrofluoride diffusion coefficient D, and the results are presented in Table 4. As previously, D was estimated taking into account the migration current contribution and the results are also shown in Table 4.

The obtained values of diffusion coefficient allow several remarks:

- they decrease when $Et_3N{\cdot}3HF$ concentration increases,
- comparison of D values determined by the two methods (influence of both the potential scan rate and angular velocity of the rotating disk electrode (Table 4), taking into account only the diffusion current) show ratios decreasing in the range from 14 to 0.5 within the $Et_3N{\cdot}3HF$ concentration examined range.
- for low $Et_3N{\cdot}3HF$ concentrations (<2×10^{-2} mol L^{-1}), the obtained diffusivities are relatively high, and that is in accordance with a 'low size' electroactive species, i.e. HF (or F^-), arising from $Et_3N{\cdot}3HF$ decomposition, especially in the diffusion layer area. Assuming that $Et_3N{\cdot}3HF$ decomposition is an equilibrium reaction, stirring could contribute to favor this equilibrium by a standardization of both the concentration and temperature especially in the diffusion area close to the electrode. For these 'low $Et_3N{\cdot}3HF$ concentrations', the determined D value must be correct because most of the introduced $Et_3N{\cdot}3HF$ decomposes, and the concentration, used to determine D (Levich slope, Table 4), is very close to its initially introduced concentration. In addition, low $Et_3N{\cdot}3HF$ concentrations lead to low current, consequently to a low fluorine quantity produced at the interface, and so a minimized effect of passivation.
- for $Et_3N{\cdot}3HF$ concentrations higher than 2×10^{-2} mol L^{-1}, the influence of stirring on the $Et_3N{\cdot}3HF$ decomposition remains low. The concentration of the electroactive species HF (or F^-), arising by $Et_3N{\cdot}3HF$ decomposition, is lower than the initial concentration of $Et_3N{\cdot}3HF$, used to estimate D, consequently, it is an apparent diffusion coefficient, and its value was assumed to be close to 1.7×10^{-9} m^2 s^{-1}.

In order to estimate $Et_3N{\cdot}3HF$ intrinsic heterogeneous electronic transfer constant $k^{0'}$, analysis of curves from Fig. 9, using the Koutecký–Levich equation, was carried out for the second triethylamine oxidation signal, located in the potential range 2/3 V vs SCE:

$$\frac{1}{I} = \frac{1}{I_k} + \frac{1}{0.62 n_{gl} F S D^{2/3} c^0 \nu^{-(1/6)} \omega^{1/2}} \quad (11)$$

where I is the current magnitude in the activation/diffusion 'potential range' of the current–potential curves (i.e. ~2.6 to ~2.8V) and I_k represents the current free of mass-transfer effects:

$$I_k = nFSck^0 \exp\left[\frac{\alpha n_{ls} F}{RT}(E - E^{0'})\right] \quad (12)$$

Results (Fig. 10) show a linear variation of $1/I = f(1/\omega^{1/2})$ for the examined potentials and for a $Et_3N{\cdot}3HF$ concentration of 2×10^{-2} mol L^{-1}. The same analysis was performed for all

Table 4
Tri-fluorinated triethylamine diffusion coefficient in acetonitrile (calculated from results of Fig. 9, using $I_{lim} = f(\omega^{1/2})$ slope for four different initial concentrations) and their comparison with the diffusion coefficient values calculated with $I_{peak} = f(r^{1/2})$ slope (Table 3).

[Et_3N•3HF] mol L^{-1}	Slope $I_{peak} = f(\omega^{1/2})$	R^2	$D_{Et_3N\cdot3HF}$ ($\times10^{10}$ m^2 s^{-1}) (without migration contribution to the current)	Estimated transference number of Et_3N·3HF, $t_{Et_3N\cdot3HF}$	$D_{Et_3N\cdot3HF}$ ($\times10^{10}$ m^2 s^{-1}) (with migration contribution to the current)	$\frac{D_{Levich}}{D_{potential\ scan\ rate}}$
8×10^{-3}	1.573×10^{-5}	0.998	17.2	0.019	16.69	14.4
2×10^{-2}	3.629×10^{-5}	0.999	15.2	0.045	14.21	8.4
3.5×10^{-2}	2.766×10^{-5}	0.986	4.4	0.074	3.89	1.9
7×10^{-2}	2.859×10^{-5}	0.999	1.6	0.130	1.32	0.6

examined concentrations; each concentration allows getting a set of parallels lines $1/I = f(1/\omega^{1/2})$, and the slope is different for each set (similar behavior to the results indicated in Table 4). The I_k determination was carried out from the intercept of these straight lines.

Analysis of the I_k values, obtained from the intercept of curves $1/I = f(1/\omega^{1/2})$, was performed according to:

$$\ln I_k = \ln(n_{gl} nFSc^0 k^{0'}) + \frac{\alpha \cdot n_{ls} \cdot F}{RT} E \quad (13)$$

where

$$k^{0'} = k^0 \exp\left[-\frac{\alpha n_{ls} F}{RT} E^{0'}\right] \quad (14)$$

Eq. (14) is the apparent intrinsic heterogeneous electronic transfer constant. Despite a certain dispersion of points, a satisfactory linear correlation of $\ln(I_k) = f(E)$ was obtained for Et_3N·3HF concentrations in the range 8×10^{-3} to 3.5×10^{-2} mol L^{-1} (results presented in Table 5).

The kinetic parameters $k^{0'}$ and αn_{ls} were calculated, and the obtained values allow some remarks:

- αn_{ls} changes with Et_3N·3HF concentration; this dispersion is mainly caused by the fact that results are very sensitive to the current magnitude: indeed, a 5% change in current values can lead to a change in the intercept of the curves $1/I = f(\omega^{1/2})$ of about 20%. This could explain the obtained ratios

$$\frac{\alpha n_{ls(Koutecký-Levich)}}{\alpha n_{ls\ potential\ scan\ rate\ Table\ 2}}$$

  in a range from 0.6 to 1.2. Nevertheless, the average value $\overline{\alpha n}_{ls} = 0.35$ is very close to the one obtained in the previous section.
- A similar variation was obtained for the apparent intrinsic heterogeneous electronic transfer constant $k^{0'}$: its values change versus

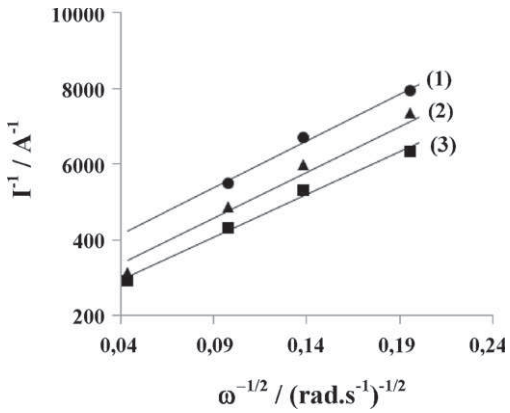

Fig. 10. Variation of the current reverse against the reverse of the angular velocity square root. Et_3N·3HF 2×10^{-2} mol L^{-1} (Fig. 9(b)). The current values are chosen for potentials in the activation/diffusion part of the I/E curve. 1–3: 2.585, 2.611 and 2.637 V vs SCE respectively. The same investigation was performed for all examined concentrations (8×10^{-3} to 7×10^{-2} mol L^{-1}).

Et_3N·3HF concentration and are very low because including the exponential term: $\exp[-(\alpha n_{ls} F/RT)E^{0'}]$ Moreover, in addition to the current sensitivity previously indicated, changes in the $k^{0'}$ values could be due to the variation of the apparent standard potential of the electroactive system (HF/F_2). $E^{0'}$ closely depends of the solution pH, which decreases because HF arises from Et_3N·3HF decomposition. Consequently, the real value of the intrinsic heterogeneous electronic transfer constant k^0 is higher than the one of $k^{0'}$. Let us note that $k^{0'}$ value 1.54×10^{-11} m s^{-1} obtained for the highest concentration is 'the most correct', or at least 'the closest' to the real value of k^0, as the apparent standard potential $E^{0'}$ is the lowest one (the lowest influence of the exponential term). In order to overcome these difficulties, and to access to more precise kinetic parameters, a possibility could be to operate electrolyses in a buffer media, for example a mixture of polar and non-polar solvents (i.e. HF + heptane). This experimental investigation will constitute a future work in order to go further to the knowledge of this system. Nevertheless current estimated value of $k^{0'}$ includes apparent standard potential $E^{0'}$ and is very useful to estimate overpotentials and consequently to perform precise energy balance for fluorination in the microreactor.

3.3. Electrochemical study of anisole on platinum anode

Electrochemical kinetic studies were carried out using a platinum disk anode, in order to understand the anisole anodic behavior, in absence and in presence of triethylamine trihydrofluoride. This study expects to help in approach the final goal of our project, 'the direct anodic fluorination of valuable adducts using an electrochemical microreactor'.

The voltammograms in Fig. 11(a), obtained for various potential scan rates, show that anisole can be oxidized for potentials higher than 1.5V vs SCE; nevertheless the curves shape is unusual. The first peak-shaped signal appears at 1.6 to 1.8V vs SCE, meanwhile for higher potentials (1.9–2.7V vs SCE), the current becomes practically constant and the curve presents a plateau. Additional anisole oxidations might take place, causing increase (instead decrease) of current magnitude.

The peak potential shifts towards more anodic values, according to a linear variation versus the scan rate logarithm (15) and confirms an irreversible anisole oxidation:

$$E_{peak} = E_a^{0'} + \frac{RT}{\alpha_a n_{ls} F}\left[0.78 + \ln\frac{D_a^{1/2}}{k_a^0} + \ln\left(\frac{\alpha_a n_{ls} F}{RT}\right)^{1/2}\right]$$
$$+1.1515\frac{RT}{\alpha_a n_{ls} F}\log(r) = 1.8551 + 0.0822\log(r) \quad R^2 = 0.997 \quad (15)$$

where k_a^0 s the anisole intrinsic heterogeneous electronic transfer constant. The curve slope allows estimation of $\alpha_a n_{ls} = 0.36$. Relation (16) illustrates a linear dependence of the potential scan rate square root on the magnitude of the 'peak'-current (i.e. potentials in

Table 5
Variation of $\ln(I_k)$ with the potential E for three $Et_3N{\cdot}3HF$ concentrations.

$[Et_3N{\cdot}3HF]$ (mol L^{-1})	$\ln(I_k) = X + Q{\cdot}E$ (relation (13))		R^2	$k^{0'}$ (m s^{-1})	αn_{ls} ($\overline{\alpha n_{ls}} = 0.35$)	$\frac{\alpha n_{ls(Koutecký-Levich)}}{\alpha n_{ls}\ \text{potential scan rate Table 2}}$
	X	Q				
8×10^{-3}	−49.799	16.436	0.986	4.86×10^{-23}	0.42	1.2
2×10^{-2}	−43.982	13.903	0.997	6.54×10^{-21}	0.35	1.1
3.5×10^{-2}	−36.883	10.793	0.996	4.52×10^{-18}	0.28	0.6

Results from Figs. 9 and 10 (and figures similar to 10, no present, for all the examined concentrations).

the range 1.65–1.85 V vs SCE), and confirms the kinetics limitation by anisole diffusion.

$$I_{peak} = 2.99 \times 10^5 \cdot n_{gl}\sqrt{\alpha_a n_{ls} D_a Sc^0}\sqrt{r} = 1.62 \times 10^{-4}\sqrt{r} \quad R^2 = 0.991 \qquad (16)$$

Diffusion coefficient of anisole D_a was estimated at $\sim 2.0 \times 10^{-8}$ m^2 s^{-1}, assuming the transferred electron number $n_{gl} = 2$, and using the curve slope as well as the previously calculated value $\alpha_a n_{ls}$. This value appears to be high for a relatively 'big sized' molecule like anisole; acetonitrile low viscosity, as well as its low ability to solvate anisole, could be one explanation for this high value. In addition, as indicate previously, the current magnitude 'captured at the peak' is higher than the expected one, because the presence of more than one oxidation steps.

In order to confirm this diffusion coefficient value, and to access to the kinetic parameters of the system, another set of experiments was carried out. Fig. 11(b) shows current–potential curves obtained at steady state for various angular velocities (ω) of the rotating platinum disk anode. The oxidation signal begins at ~1.6 V vs SCE and is followed by a diffusion plateau, presenting a limiting current (mainly for $\omega < 1000$ rpm). For higher angular velocities, the current magnitude reaches a maximum in a potential range from 2 to 2.2 V vs SCE, and decreases for more anodic potentials. A strong stirring leads to a current increase and consequently, more important quantities of anisole are involved into the reaction close to the interface. In these conditions, partial electrode passivation can occur and the current decreases.

Using the maximum current as an approximation for the expected limiting current (Fig. 11(b)), and applying the Levich relation (10), a non-linear correlation of $I_{lim} = f(\omega^{1/2})$ is obtained within the ω examined range (Fig. 12(a)), in accordance with the previous passivation explanations. However, for low angular velocities (ω lower than 1000 rpm), passivation effects are reduced and a linear correlation of $I_{lim} = f(\omega^{1/2})$ is obtained (17).

$$I_{lim}\,(A) = 8.82 \times 10^{-6}\omega^{1/2}\,(\text{rad s}^{-1})^{0.5},$$
$$R^2 = 0.9999 \quad (100 \le \omega \le 500\,\text{rpm}) \qquad (17)$$

Anisole diffusion coefficient deduced from the slope is $D_a \sim 1.6 \times 10^{-8}$ m^2 s^{-1} (assuming $n_{gl} = 2$) a value that seems to be more precise than the previous one, because the low passivation effects at low stirring rates.

Analysis of curves in Fig. 11(b) was carried out using the Koutecký–Levich Eq. (11), by plotting the variation of the current reverse against the reverse of the angular velocity square root. The current was captured in the activation/diffusion range of current–potential curves, for potentials from 1.7 to 1.75 V vs SCE, and results (Fig. 12(b)), show a linear variation of $1/I = f(1/\omega^{1/2})$ for the four examined potentials.

Logarithmic analysis of the obtained I_k values (from the intercept of curves Fig. 12(b)) versus the anodic potential, according to relation (13), allows determination of the kinetic parameters $k_a^{0'}$ and $\alpha_a n_{ls}$ and results show a linear correlation (18).

$$\ln(I_k) = 15.144E - 12.241 \quad R^2 = 0.994 \qquad (18)$$

where $\alpha_a n_{ls} = 0.39$ and $k_a^{0'} = k^0 \exp\left[\frac{-(a_a n_{ls} F)}{RT}E^{0'}\right] \sim 8 \times 10^{-6}$ m s^{-1}.

The apparent intrinsic heterogeneous electronic transfer constant ($k_a^{0'}$) value is low, indicating an irreversible behavior for anisole oxidation. However, a rigorous analysis requiring additional investigations to calculate the apparent standard potential $E^{0'}$ of the system, has to be carried out in order to obtain the intrinsic heterogeneous electronic transfer constant (k^0). For the pursuit of the fluorination within a microreactor of adducts like anisole the $k_a^{0'}$ value will be used.

3.4. Electrochemical study of anisole/triethylamine trihydrofluoride mixture on platinum anode and preliminary set of fluorination

The main goal of this part of the study is to understand the electrochemical behavior of the system anisole/triethylamine trihydrofluoride before approaching the anisole fluorination within an electrochemical microreactor. Because the triethylamine trihydrofluoride is used as a fluorinating agent as well as an electrolyte, its concentration will be higher (8×10^{-3} mol L^{-1}) than anisole concentration (10^{-3} mol L^{-1}).

Current–potential curves, obtained by varying both the potential scan rate (Fig. 13(a)) and the angular velocity of the rotating disk electrode (Fig. 13(b)), show the presence of three distinct signals, in the potential ranges 1–1.6 V, 1.7–1.9 V and 2–2.6 V vs SCE respectively.

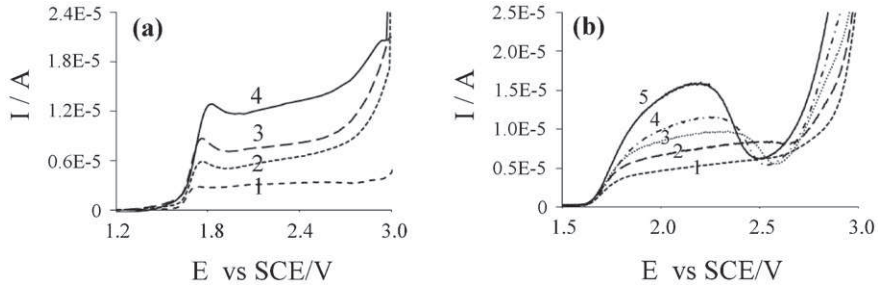

Fig. 11. Current–potential curves obtained on platinum rotating disk ($r = 1$ mm), immersed in acetonitrile solvent containing anisole 10^{-3} mol L^{-1} and Bu_4NClO_4 0.2 mol L^{-1}; CE: Pt; 25 °C. (a) Curves plotted at different potential scan rates; no stirring. 1–4: 0.017, 0.083, 0.170 and 0.500 V s^{-1} respectively, and (b) curves plotted at different angular velocities; $r = 4 \times 10^{-3}$ V s^{-1}. 1–5: 100, 250, 500, 1000 and 3500 rpm respectively.

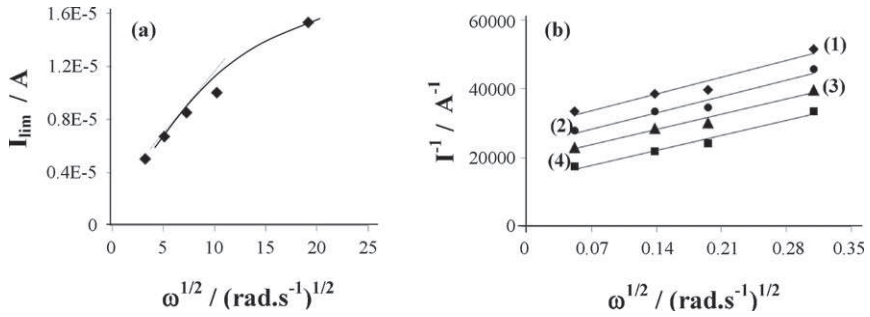

Fig. 12. Angular velocity dependence on the anisole oxidation current; results obtained from Fig. 11(b). (a) Limiting current variation against the square root of the angular velocity for anisole oxidation; and (b) variation of current reverse against the reverse of the angular velocity square root. The current was captured in the activation/diffusion range of the *I*/*E* curve. 1–4: 1.702, 1.712, 1.725 and 1.751 V vs SCE, respectively.

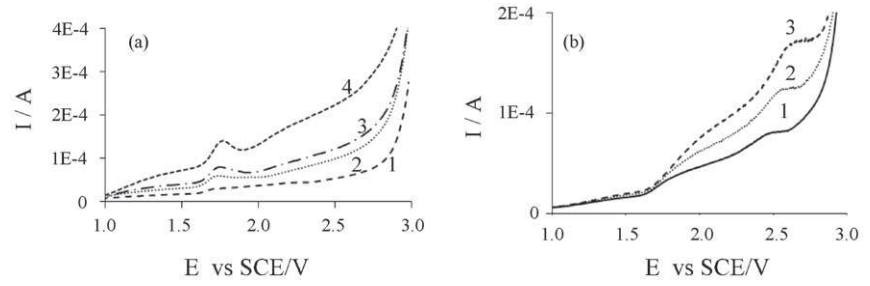

Fig. 13. Current–potential curves obtained on platinum rotating disk ($r = 1$ mm), immersed in acetonitrile solvent containing anisole 10^{-3} mol L^{-1}, $Et_3N{\cdot}3HF$ 8×10^{-3} mol L^{-1} and Bu_4NClO_4 0.2 mol L^{-1}; CE: Pt; 25 °C; no stirring. (a) Different potential scan rates, 1–4: 0.017, 0.083, 0.170 and 0.500 V s^{-1} respectively, and (b) different angular velocities, 1–3: 100, 250 and 500 rpm respectively; $r = 4 \times 10^{-3}$ V s^{-1}.

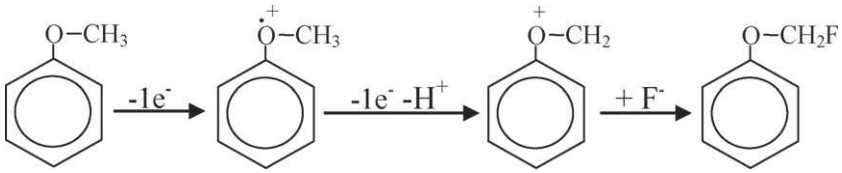

Fig. 14. Reaction mechanism proposed for anisole electro-fluorination.

These voltammograms correspond to the addition of triethylamine trihydrofluoride and anisole oxidation curves. The second signal (1.7–1.9 V) was attributed to anisole oxidation, while the first (1–1.6 V) and the third (2–2.6 V) were attributed to the triethylamine trihydrofluoride.

The current magnitude for the triethylamine trihydrofluoride oxidation in presence of anisole seems to be lower than the current magnitude for the triethylamine trihydrofluoride alone. Indeed, a comparison of these currents for curves obtained in the same conditions (no. 3 Fig. 13(b), $I \sim 1.71 \times 10^{-4}$ A and no. 3 Fig. 9(a), $I \sim 1.31 \times 10^{-4}$ A) shows significant differences. An explanation could be that anisole oxidation leads to cation radicals that are further reacting with triethylamine trihydrofluoride (or fluoride). This could be in accordance with the reaction mechanisms proposed by Hou and Fuchigami [3] for dimethoxyethane (Fig. 14).

When operating with anisole alone, for relatively strong stirring rates, its oxidation to cation radicals seems leading to a partial anode passivation, causing a decrease in the current magnitude (Fig. 11(b)). The passivation seems to disappear when triethylamine trihydrofluoride is present, probably because of the electrore-generated radicals consumption, avoiding their duplication and consequently the electrode passivation. This fact allows us to pursue in the designing of the electrofluorination process without need of a special attention to the passivation problems.

This study shows that for anisole electro-fluorination it is important to maintain the anodic potential at 2.2–2.3 V vs SCE during fluorination, in order to avoid tri-fluorinated triethylamin oxidation to gaseous fluorine. A preliminary set of experiments was performed using a filter-press electrochemical microreactor [18,19] in order to fluorinate both anisole and dimethoxyethane in various working conditions ($-10\,°C < T < 40\,°C$). The results did not show anisole fluorination (either on the aromatic ring nor the methoxy group). Nevertheless, dimethoxyethane was 'mono-fluorinated' (which seems to be more difficult than anisole fluorination) and two reaction products were obtained ($FCH_2OCH_2CH_2OCH_3$ chemical yield: 62% and $CH_3OCHFCH_2OCH_3$ chemical yield: 38%), when a charge of 7F/mole was used. A more important investigation of the fluorination of anisole will constitute the goal of future works.

4. Conclusions

The aim of this preliminary study was to examine the electrochemical behavior of anisole and triethylamine trihydrofluoride (fluorinating agent) in order to help to approach the final goal of our study, the direct anodic fluorination of valuable adducts using an electrochemical microreactor.

Several kinetic studies, performed in various conditions, show that both compounds can be oxidized. Triethylamine trihydrofluoride 'doubly' reacts, under both adsorbed and free forms, at two different potentials. Adsorption is governed by the Langmuir model, with an adsorption equilibrium constant $K = (0.8 \pm 0.2) \times 10^2$ estimated at 25 °C and indicating a relatively low affinity of the triethylamine trihydrofluoride for the platinum anode.

One signal was observed for anisole oxidation, even if more than one reaction seems to occur. Electrode passivation, observed during anisole oxidation, disappear in presence of triethylamine trihydrofluoride, phenomena that could be an important advantage for the fluorination process.

Triethylamine trihydrofluoride diffusion coefficient within the working media, determined by two different ways ($1.2 \times 10^{-10} < D$ ($m^2\ s^{-1}$) $< 1.7 \times 10^{-9}$), appears to be 'high' and varies versus the triethylamine trihydrofluoride initial concentration in the examined range (8×10^{-3}–3.5×10^{-2} mol L^{-1}). One can propose for $Et_3N{\cdot}3HF$, an apparent diffusion coefficient values close to $1.7 \times 10^{-9}\ m^2\ s^{-1}$, determined for the lowest Triethylamine trihydrofluoride concentrations involved in this study.

Anisole diffusion coefficient was estimated by two methods and similar results were obtained: ($1.6 \times 10^{-8} < D (m^2\ s^{-1}) < 2.0 \times 10^{-8}$). As for $Et_3N{\cdot}3HF$, anisole diffusion coefficient is relatively high for a relatively 'big sized' molecule and it could be justified by low acetonitrile viscosity.

Some kinetic parameters ($\overline{\alpha n_{ls}}$ and $k^{0'}$) of both anisole and triethylamine trihydrofluoride were also proposed. For the anodic electronic transfer coefficient, in the case of both anisole and triethylamine trihydrofluoride, results led to the same and reproducible value: $\overline{\alpha n_{ls}} \sim 0.36$ validated by two different study methods.

Though, the value of the intrinsic heterogeneous electronic transfer constant (k^0) could not be calculated, because it requires additional investigations ($E^{0'}$ of these systems). However, results show some values of the apparent intrinsic heterogeneous electronic transfer constant for both anisole ($k_a^{0'} \sim 8 \times 10^{-6}$ m s^{-1}) and triethylamine trihydrofluoride ($k_a^{0'}$ in the range 4.86×10^{-23} to 4.52×10^{-18} m s^{-1}). These values are low (even if they contain an exponential term of the standard potential), indicating irreversible systems; for triethylamine trihydrofluoride, the obtained value is very low and varies with concentration, because the pH modification caused by the triethylamine trihydrofluoride decomposition.

Preliminary results of preparative electrolyses, carried out in conditions defined by the electrochemical kinetic study, are encouraging [18,19], especially for fluorination of dimethoxymethane, demonstrating that electro-fluorination can be performed in the alpha position of a heteroatom.

Acknowledgement

We would like to thank Maria Pilar García León for her contributions and very helpful discussions.

References

[1] V. Suryanarayanan, M. Noel, Journal of Fluorine Chemistry 92 (1998) 177; N. Ilayaraja, M. Noel, Journal of Electroanalytical Chemistry 638 (2010) 39.
[2] Y. Hou, T. Fuchigami, Electrochemistry Communications 1 (1999) 445.
[3] Y. Hou, T. Fuchigami, Tetrahedron Letters 40 (1999) 7819.
[4] Y. Hou, S. Higashiya, T. Fuchigami, Journal of Organic Chemistry 64 (1999) 3346.
[5] D. Baba, H. Ishii, S. Higashiya, K. Fujisawa, T. Fuchigami, Journal of Organic Chemistry 66 (2001) 7020.
[6] K. Suzuki, H. Ishii, T. Fuchigami, Tetrahedron Letters 42 (2001) 4861.
[7] K.M. Dawood, T. Fuchigami, Tetrahedron Letters 42 (2001) 2513.
[8] H. Ishii, Y. Hou, T. Fuchigami, Tetrahedron Letters 56 (2000) 8877.
[9] N. Ilayaraja, M. Noel, Journal of Electroanalytical Chemistry 632 (2009) 45.
[10] N. Ilayaraja, S. Radhakrishnan, N.G. Renganathan, Chemistry and Materials Science 16 (2010) 137.
[11] H. Löwe, W. Ehrfeld, Electrochimica Acta 44 (1999) 3679.
[12] W. Ehrfeld, V. Hessel, H. Lehr, Chemistry and Materials Science 194 (1998) 233.
[13] N. de Mas, A. Gunther, M.A. Schmidt, K.F. Jensen, Industrial Engineering and Chemical Research 48 (2009) 1428.
[14] B.A. Shainyan, Y.S. Danilevich, Russian Journal of Organic Chemistry 42 (2006) 231.
[15] J.S. Jaworski, M. Cembor, M. Orlik, Journal of Electroanalytical Chemistry 582 (2005) 165.
[16] G. Dabosi, M. Martineau, G. Durand, Analysis 6 (1978) 289.
[17] A.J. Bard, L.R. Faulkner, Electrochemical Methods, Fundamentals and applications, 2nd ed., John Wiley & Sons Inc., New York, 2001.
[18] C. Kane, T. Tzedakis, AIChE Journal 54 (2008) 365.
[19] T. Tzedakis, C. Kane, A. Launay. 'Microréacteur'. French patent no. 04.12305, 2004, PCT 2006, No. WO 2006/053962; extended to USA 01 12 2004 no. 60/631,877.